RESEARCH ARTICLE

Spatial patterns in CO_2 evasion from the global river network

Ronny Lauerwald[1,2,3], Goulven G. Laruelle[1,4], Jens Hartmann[3], Philippe Ciais[5], and Pierre A. G. Regnier[1]

[1]Department of Earth and Environmental Sciences, Université Libre de Bruxelles, Brussels, Belgium, [2]Institut Pierre-Simon Laplace, Paris, France, [3]Institute for Geology, University of Hamburg, Hamburg, Germany, [4]Department of Earth Sciences-Geochemistry, Utrecht University, Utrecht, Netherlands, [5]LSCE IPSL, Gif Sur Yvette, France

Abstract CO_2 evasion from rivers (FCO_2) is an important component of the global carbon budget. Here we present the first global maps of CO_2 partial pressures (pCO_2) in rivers of stream orders 3 and higher and the resulting FCO_2 at 0.5° resolution constructed with a statistical model. A geographic information system based approach is used to derive a pCO_2 prediction function trained on data from 1182 sampling locations. While data from Asia and Africa are scarce and the training data set is dominated by sampling locations from the Americas, Europe, and Australia, the sampling locations cover the full spectrum from high to low latitudes. The predictors of pCO_2 are net primary production, population density, and slope gradient within the river catchment as well as mean air temperature at the sampling location ($r^2 = 0.47$). The predicted pCO_2 map was then combined with spatially explicit estimates of stream surface area A_{river} and gas exchange velocity k calculated from published empirical equations and data sets to derive the FCO_2 map. Using Monte Carlo simulations, we assessed the uncertainties of our estimates. At the global scale, we estimate an average river pCO_2 of 2400 (2019–2826) μatm and a FCO_2 of 650 (483–846) Tg C yr^{-1} (5th and 95th percentiles of confidence interval). Our global CO_2 evasion is substantially lower than the recent estimate of 1800 Tg C yr^{-1} although the training set of pCO_2 is very similar in both studies, mainly due to lower tropical pCO_2 estimates in the present study. Our maps reveal strong latitudinal gradients in pCO_2, A_{river}, and FCO_2. The zone between 10°N and 10°S contributes about half of the global CO_2 evasion. Collection of pCO_2 data in this zone, in particular, for African and Southeast Asian rivers is a high priority to reduce uncertainty on FCO_2.

1. Introduction

Following several syntheses published over the last decade [*Cole et al.*, 2007; *Battin et al.*, 2009; *Tranvik et al.*, 2009; *Aufdenkampe et al.*, 2011], inland waters (streams, rivers, lakes, and reservoirs) are presented in the fifth assessment report of the Intergovernmental Panel on Climate Change [*Ciais et al.*, 2013] as an active component of the global carbon cycle with substantial net evasion of CO_2 (FCO_2) to the atmosphere. This is a major paradigm shift from earlier assessments, which represented inland waters as a passive conduit of carbon from land to ocean [*Denman et al.*, 2007], though inland waters were already known to be net sources of CO_2 to the atmosphere [e.g., *Kempe*, 1982]. Published global estimates of FCO_2 vary nevertheless substantially, and the quantitative contribution of inland waters to the atmospheric CO_2 budget has large uncertainties [*Regnier et al.*, 2013]. Reported values of FCO_2 for the fluvial network alone range from 0.26 Pg C yr^{-1} to 1.8 Pg C yr^{-1} [*Richey et al.*, 2002; *Cole et al.*, 2007; *Tranvik et al.*, 2009; *Aufdenkampe et al.*, 2011; *Regnier et al.*, 2013; *Raymond et al.*, 2013], the latest published estimate (1.8 Pg C yr^{-1}) [*Raymond et al.*, 2013] being about twice as large as the lateral export of carbon to the coastal ocean from the global river network (see the reviews by *Bauer et al.* [2013] and *Regnier et al.* [2013]).

However, even the most recent assessments of FCO_2 do not resolve well its important spatial variability. So far, extrapolations of field data were performed to achieve a lumped global estimate [*Cole et al.*, 2007], a segmentation according to three latitudinal zones (tropical, temperate, and boreal to arctic) [*Aufdenkampe et al.*, 2011], and a regionalization based on the COSCAT units of *Meybeck et al.* [2006] [*Raymond et al.*, 2013]. This study takes the next step forward and resolves FCO_2 at a much higher resolution of 0.5°. This makes our estimation directly comparable to typical outputs of global land surface models such as ecosystem productivity and terrestrial carbon stocks.

A major challenge for achieving a spatially explicit assessment of river FCO_2 at half a degree resolution is the uneven coverage of water chemistry data (alkalinity, pH, and water temperature) required for the upscaling

of the river pCO_2 on a grid over the entire globe and, subsequently, of FCO_2. While some rivers in industrialized countries are covered by a dense network of sampling locations, a very large fraction of the global river network remains only sparsely or not at all surveyed [*Regnier et al.*, 2013]. Thus, suitable interpolation techniques are required to fill the numerous spatial gaps that appear at the targeted resolution of half a degree and the uncertainty due to the limited sampling needs to be quantified. In a continental scale study over North America, it was shown that the river pCO_2 can, to some extent, be estimated from high-resolution geodata representing the major environmental controls of the CO_2 exchange between rivers and the atmosphere [*Lauerwald et al.*, 2013]. In this study, we expand this approach to derive empirical equations that allow us to predict the spatial distribution of pCO_2 and FCO_2 from rivers of stream orders 3 and higher at the global scale on a 0.5° grid. In addition, a Monte Carlo analysis is applied to our empirical predictors to quantify the uncertainties in pCO_2 and FCO_2 estimations which were not considered in earlier studies.

2. Methods

The global river chemistry database GloRiCh [*Hartmann et al.*, 2014] (section 2.1.1), which was already used by *Raymond et al.* [2013], and geodata on river catchment properties were used to derive a functional relationship between river pCO_2 and environmental variables. The resulting prediction model was then applied to derive a global 0.5° map of yearly averaged river pCO_2 (section 2.1.2). This map was used in combination with spatially resolved estimates of gas exchange velocity k and surface lake and stream water area A_{river} to calculate FCO_2 from the global river network at the same resolution (section 2.2). Using Monte Carlo simulations, we quantified the uncertainty of our estimates (section 2.3).

2.1. River pCO_2
2.1.1. Calculation of River pCO_2 From Observed Data

Using PhreeqC v2 [*Parkhurst and Appelo*, 1999], we calculated 101×10^3 pCO_2 values from alkalinity, pH, water temperature, and, where available, concentrations of major inorganic solutes reported in the hydrochemical database GloRiCh [*Hartmann et al.*, 2014]. Data were selected according to the following criteria: (1) The delineation of the catchment of the sampling location is available in GloRiCh; (2) The sample dates from 1990 or later to avoid the high river pollution period in Europe; (3) Samples with a pH lower than 5.4 (1.7% of the considered water samples) are discarded because calculating pCO_2 from alkalinity and pH is highly error prone in low-pH waters [*Raymond et al.*, 2013], mainly due to contributions of noncarbonate alkalinity [*Hunt et al.*, 2011]; (4) In order to calculate robust averages of pCO_2, only sampling locations were retained where monthly median pCO_2 values could be calculated from at least three single values and without leaving gaps of more than three consecutive months without a median pCO_2 value. Given the small number of data for each location month, the median was preferred over the mean to limit the effect of single, probably erroneous outliers. To ensure an equilibrated seasonal weighting, gaps in the seasonal cycle were closed by linear interpolation between the previous and next following median monthly pCO_2 values [cf. *Lauerwald et al.*, 2013]. Prior to calculation of annual average pCO_2 values, the months for which it can be assumed that contributions to annual CO_2 evasion are negligible were discarded. This corresponds to months of seasonal river drying (i.e., monthly runoff is zero) or ice cover (i.e., the average monthly air temperature is below −4.8°C, see section 2.2).

The data set matching the above selection criteria corresponds to 1162 sampling locations. Albeit not completely fulfilling these conditions, in particular, the requirement of three values per month, 21 additional sampling locations located in climate zones so far underrepresented in the analysis were incorporated in the analysis. This includes data from the research projects CAMREX (Carbon in the Amazon River Experiment) [*Richey et al.*, 1990] (Amazon Basin), PARTNERS [*PARTNERS-Project-Group*, 2009] (large Artic Rivers), and a part of ORE-HYBAM [*Cochonneau et al.*, 2006] (Amazon Basin and smaller catchments in Guyana). In this case, we verified manually all pCO_2 entries to avoid unrealistic values that would add noise to monthly averages. In contrast to most GloRiCh data, the pH reported in these research programs has a precision of two decimal places, which increases the precision of the calculated pCO_2. Although the samples from the CAMREX project date from the 1980s, the sampling locations are far from anthropogenic point sources, and we kept them in the upscaling under the premise that they are representative of
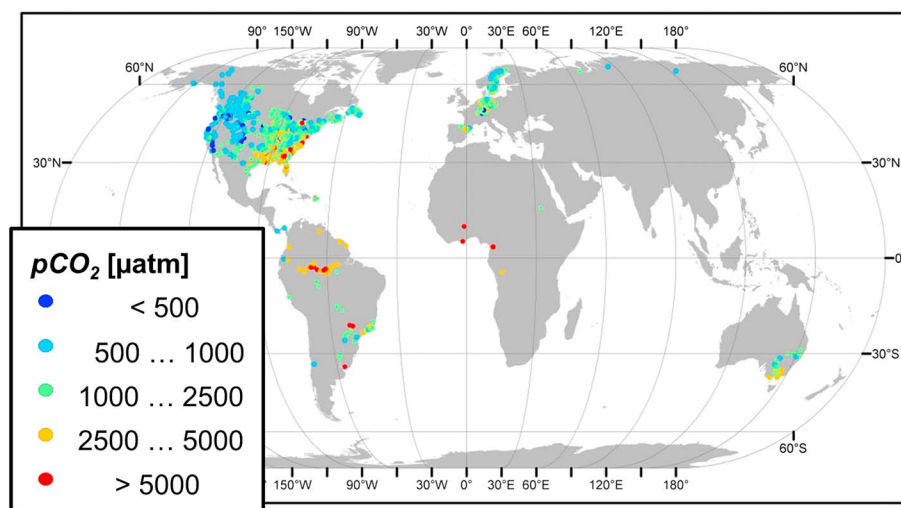
Figure 1. Average pCO_2 per sampling location used for statistical analysis ($n = 1182$).

present-day conditions. Altogether, 1182 sampling locations were thus retained, which represent 17.6% of the sampling locations used in the study of *Raymond et al.* [2013]. While *Raymond et al.* [2013] calculated a median pCO_2 per COSCAT region from the bulk of pCO_2 values therein—including values from sampling locations with only single or few values—we aimed at calculating robust average pCO_2 values per sampling location and had thus to exclude the major part of the data set. The retained sampling locations are unevenly distributed around the globe. Most of them (727) are distributed over North and South America, where they cover nearly all latitudes (Figure 1). Another significant fraction (402) is concentrated in Europe, the remaining sites (53) being distributed over Australia, tropical Africa, and the Northern rim of Asia. Although large areas on the continents are only sparsely sampled, a wide variety of climates which is required to train a global empirical model of river pCO_2 is covered (see the statistical distribution of climatic variables in Table 1).

Table 1. Environmental Parameters Evaluated as Potential Predictors of Average pCO_2 of River Water[a]

			Statistics for Training Catchments				
Parameter	Units	Mean	Median	Min	Max	Source	Resolution
		Parameters Referring to River Catchment					
Slope gradient	Degrees	2.061	1.367	0.036	15.115	*GLOBE-Task-Team et al.* [1999]	30″
Area	m^2	7.14×10^{10}	$2.09 \ 10^9$	4.76×10^6	4.70×10^{12}	Derived from routing scheme (section 2)	
NPP	g C m^{-2} yr^{-1}	536	532	0	1641	*Zhao et al.* [2005]	30″
Pop. density ('00)	Inh. km^{-2}	125.6	42.7	0.0	2337.6	*CIESIN, and CIAT* [2005]	2.5′
Lake area proportion	1	0.008	0.002	0.000	0.339	*Lehner and Döll* [2004]	
Runoff	mm yr^{-1}	384	309	0.01	2707	*Fekete et al.* [2002]	30′
Permafrost index	Index	0.011	0.000	0.000	0.933	*Gruber* [2012]	30″
Flooded proportion	1	0.043	0.014	0.000	0.662	*Prigent et al.* [2007]	15′
Air temperature	°C	10.4	9.0	2.6	28.0	*Hijmans et al.* [2005]	30″
Precipitation	mm yr^{-1}	925	816	257	3132	*Hijmans et al.* [2005]	30″
Evaporation	mm yr^{-1}	54	48	2	123	*Miralles et al.* [2011]	15′
		Parameters Referring to Sampling Location					
Flooded proportion	1	0.073	0.022	0.000	0.799	*Prigent et al.* [2007]	15′
Air temperature	°C	12.16	10.37	0.57	29.43	*Hijmans et al.* [2005]	30″
Precipitation	mm yr^{-1}	865	766	12	3370	*Hijmans et al.* [2005]	30″
Evaporation	% of Precipitation	53	47	5	132	*Miralles et al.* [2011]	15′
Altitude	m	319	190	1	3006	*GLOBE-Task-Team et al.* [1999]	30″
Strahler order		4	4	0	10	Derived from routing scheme (section 2)	
Latitude	Degrees	38.1	44.6	−38.3	69.4	GloRiCh data base	

[a]Statistical distribution of the parameters within the training set of sampling locations and the related river catchments; values refer to units indicated in second column.

Table 2. Correlation Between Average pCO$_2$ and Different Environmental Parameters[a]

	log$_{10}$ (Slope Gradient)	log$_{10}$ (Area)	Net Primary Production	sqrt (Population Density)	sqrt (Lake Area Prop.)	Runoff	Permafrost Index	sqrt (Flooded Prop.)	Mean Air Temperature
				Parameters Referring to River Catchment					
log$_{10}$(pCO$_2$)	−0.55	−0.06	0.32	0.26	−0.15	n.s.	−0.21	0.22	0.51
				Parameters Referring to River Catchment					
log$_{10}$(Slope gradient)		0.10	−0.06	−0.14	n.s.	0.19	0.24	−0.47	−0.41
log$_{10}$(Area)			n.s.	−0.31	0.32	−0.07	0.10	−0.11	0.28
Net primary production				−0.08	−0.13	0.27	−0.25	−0.19	0.45
sqrt(Pop. density)					−0.18	n.s.	−0.18	0.25	n.s.
sqrt(Lake area prop.)						0.09	n.s.	0.26	−0.11
Runoff							n.s.	0.09	0.09
Permafrost Index								−0.09	−0.18
sqrt(Flooded prop.)									0.11
Mean air temperature									
Precipitation									
Evaporation									
				Parameters Referring to Sampling Location					
sqrt(Flooded prop.)									
Mean air temperature									
Precipitation									
Evaporation									
log$_{10}$(Altitude)									
Strahler order									

[a]Reported are Pearson correlation coefficients which are statistically significant ($p < 0.05$); n.s. means not significant.

2.1.2. Upscaling of pCO$_2$ Data

For each sampling location, catchment properties were calculated in ArcGIS 10 [see *Lauerwald et al.*, 2013 for details]. The delineation of the watersheds was taken from GloRiCh and is based on the hydrologic routing schemes Hydrosheds (15 arcsec) [*Lehner et al.*, 2008] and Hydro1k (1 km), which were also used for the spatially explicit estimation of riverine pCO$_2$ in this study. These schemes, designed to be used in hydrological modeling, consist in a set of digital elevation models (DEM) and their associated flow direction grids. Hydrosheds was derived from the Shuttle Radar Topography Mission DEM, and its coverage is limited to latitudes south of 60°N. For higher latitudes, we used Hydro1K derived from the DEM GTOPO30 [U.S. Geological Survey] as an alternative. More manpower has however been invested on ground-truth checks and correction of flow directions for Hydrosheds [*Lehner et al.*, 2008]. Therefore, in addition to its lower resolution, Hydro1k provides a less accurate representation of the natural stream network and its use was thus restricted to areas not covered by Hydrosheds. Table 1 lists the environmental variables attributed to each sampling location or river catchment and the geodata sets from which they were extracted. A short description and evaluation of each data set can be found in the supporting information.

We analyzed the correlations between the different environmental variables and between environmental variables and average pCO$_2$ per sampling location (Table 2). We transformed some of the variables and pCO$_2$ to account for skewed distributions and nonlinear correlations. The pCO$_2$, the altitude of the sampling location and the average slope gradient of the river catchment were expressed as logarithms (log$_{10}$). For population density and areal proportion of inundated areas and lakes, we used square roots instead of logarithms, because these parameters often show a value of 0.

We used multilinear regression to derive a prediction equation for log$_{10}$(pCO$_2$) as a function of the (transformed) environmental variables. A stepwise backward algorithm implemented in the software package STATISCA™ V 8 was applied to identify a suitable, nonredundant set of environmental variables as predictors for pCO$_2$. Redundancies typically occur when some of the variables are highly intercorrelated (colinearity). The stepwise backward algorithm retained the four predictors: average slope gradient, net primary production (NPP), population density within the river catchment, and mean air temperature at the sampling location (Table 3). The residuals of the regression function (observed-predicted values) do not show any significant correlations with any of the discarded predictors. The fitted regression equation was

Table 2. (continued)

Parameters Referring to River Catchment		Parameters Referring to Sampling Location						
Precipitation	Evaporation	sqrt (Flooded Prop.)	Mean Air Temperature	Precipitation	Evaporation	$\log_{10}$ (Altitude)	Strahler Order	Absolute Latitude
0.32	0.39	0.25	0.34	0.34	0.40	−0.37	n.s.	−0.34
		Parameters Referring to River Catchment						
−0.12	−0.28	−0.36	−0.14	−0.22	−0.32	0.42	0.10	0.13
n.s.	0.07	0.15	0.46	n.s.	0.07	−0.13	0.97	−0.33
0.62	0.61	−0.07	0.35	0.51	0.56	−0.19	n.s.	−0.44
n.s.	−0.06	0.15	−0.15	n.s.	n.s.	−0.14	−0.29	0.13
n.s.	−0.08	0.16	n.s.	n.s.	−0.08	−0.14	0.31	0.10
0.68	0.39	0.13	0.08	0.61	0.36	−0.18	n.s.	−0.21
−0.16	−0.22	n.s.	−0.13	−0.13	−0.19	0.11	0.09	0.21
0.14	0.09	0.73	n.s.	0.17	0.12	−0.40	−0.11	n.s.
0.62	0.78	0.24	0.91	0.61	0.75	−0.35	0.26	−0.86
	0.85	0.21	0.53	0.91	0.82	−0.34	n.s.	−0.66
		0.14	0.68	0.80	0.95	−0.30	0.06	−0.78
		Parameters Referring to Sampling Location						
			0.18	0.25	0.16	−0.46	0.15	−0.16
				0.51	0.64	−0.22	0.43	−0.91
					0.86	−0.37	n.s.	−0.63
						−0.33	n.s.	−0.74
							−0.13	0.14
								−0.30

then applied in ArcGIS 10 to calculate spatially explicit estimates of river pCO_2 from the selected predictors at the high resolution of the routing schemes. For the generation of the global pCO_2 map, these estimates were spatially aggregated to the 0.5° resolution, using a weighted averaging procedure, scaling each high-resolution pCO_2 value to the corresponding effective stream surface area $A_{river,eff}$ (see section 2.2)

2.2. FCO_2 Calculation

FCO_2 was calculated from the water-atmosphere CO_2 gradient ΔCO_2, the effective water surface area through which this flux takes place ($A_{river,eff}$), and the gas exchange velocity k (equation (1)). In order to produce spatially explicit estimates of FCO_2, we calculated spatial representations of the annual averages for these three factors. FCO_2 was first calculated at the high resolution of the routing schemes (15 arcsec for Hydrosheds and 1 km for Hydro1k), using estimates of river pCO_2, $A_{river,eff}$, and k at the same resolution. These high-resolution FCO_2 maps were then aggregated to 0.5° resolution, which corresponds to the resolution of the coarsest input data (the UNH/GRDC runoff data). For all geocomputational work we used ArcGIS 10 from ESRI™.

$$FCO_2 = A_{river,eff} \cdot k \cdot \Delta CO_2 \tag{1}$$

ΔCO_2 was calculated from the difference between the estimated pCO_2 of river water (section 2.1) and the pCO_2 of the atmosphere, converted to CO_2 concentrations using Henry's constant KCO_2 (equation (2)). We assumed an atmospheric pCO_2 of 390 μatm and calculated KCO_2 at the estimated in situ water

Table 3. Retained Predictors With b Estimates, Associated Standard Errors, and Partial Correlations to the Dependent Variable $\log_{10}(pCO_2 \text{ [atm]})$[a]

Predictor	b Estimate	Standard Error	t(1176)	P Value	Partial Correlation
Intercept	−3.192	0.021	−151.531	0.000	
sqrt(Pop. Density [km^{-2}]) × 10^{-3}	9.372	0.807	11.616	0.000	0.321
$\log_{10}$(Slope gradient [°])	−0.279	0.013	−21.479	0.000	−0.531
T_{air}[b] at location [10^{-2} °C]	1.343	0.128	10.506	0.000	0.293
NPP[c] [10^{-3} g C m^{-2} yr^{-1}]	0.279	0.028	9.872	0.000	0.277

[a]With the exception of T_{air}, all predictors refer to the river catchment.
[b]T_{air} stands for mean air temperature.
[c]NPP stands for net primary production.

temperature T_{water} using the equation proposed by *Telmer and Veizer* [1999]. Monthly values of T_{water} were calculated from average monthly air temperature at the sampling location T_{air} (equation (3)), using a linear regression equation derived from 498×10^3 pairs of observed T_{water} (GloRiCh data base) and T_{air} values [*Hijmans et al.*, 2005].

$$\Delta CO_2 = KCO_2 \cdot \left(pCO_2 - pCO_{2atmosphere}\right) \tag{2}$$

$$T_{water}[°C] = 3.941 \pm 0.007 + 0.818 \pm 0.0004 \cdot T_{air}[°C] \quad (R^2 = 0.88) \tag{3}$$

The spatially explicit calculations of stream surface area A_{river} and gas exchange velocity k depend on river discharge. We calculated average annual river discharge Q_{ann} from the UNH/GRDC runoff data and routed the flow using Hydrosheds or Hydro1K. We then used the two empirical equations from *Raymond et al.* [2012, 2013] to derive two estimates of both stream width B and stream flow velocity v from Q_{ann} (equations (4)–(7)). Distinct values of A_{river} were calculated from each estimated stream width and stream length per grid cell. The latter was extracted from a representation of the stream network which uses a threshold on the minimum catchment area of $10\,km^2$. This threshold was chosen to ensure that the stream networks derived from Hydrosheds and Hydro1k are comparable. Parts of the stream network overlapping with lakes and reservoirs extracted from the data set by *Lehner and Döll* [2004] were removed. The effective river surface area $A_{river,eff}$ was calculated from A_{river} by taking into account inhibition of gas exchange during periods of ice cover and stream drying. Equation (3) predicts negative water temperature when average monthly air temperatures are below $-4.8°C$. Accordingly, we assumed ice cover for the months with lower average air temperature, a procedure which is broadly consistent with that of *Raymond et al.* [2013]. We assumed stream drying for months during which the monthly discharge $Q_{month} = 0\,m^3\,s^{-1}$. Seasonal stream drying of ephemeral streams is widely found in semiarid regions, like, for instance, the Arroyos in the south western U.S.

$$\ln(B[m]) = 2.56 + 0.423 \cdot \ln\left(Q_{ann}[m^3\,s^{-1}]\right) \qquad [\text{after } Raymond\ et\ al., 2012] \tag{4}$$

$$\ln(B[m]) = 1.86 + 0.51 \cdot \ln\left(Q_{ann}[m^3\,s^{-1}]\right) \qquad [\text{after } Raymond\ et\ al., 2013] \tag{5}$$

$$\ln\left(v\,[m\,s^{-1}]\right) = -1.64 + 0.285 \cdot \ln\left(Q_{ann}[m^3\,s^{-1}]\right) \qquad [\text{after } Raymond\ et\ al., 2012] \tag{6}$$

$$\ln\left(v[m\,s^{-1}]\right) = -1.06 + 0.12 \cdot \ln\left(Q_{ann}[m^3\,s^{-1}]\right) \qquad [\text{after } Raymond\ et\ al., 2013] \tag{7}$$

$$k_{600}[m\,d^{-1}] = v[m\,s^{-1}] \cdot S_{chan}[1] \cdot 2841 + 2.02 \qquad [\text{after } Raymond\ et\ al., 2012] \tag{8}$$

where B is the stream width, Q_{ann} is the annual average discharge, v is the stream flow velocity, and S_{chan} is the channel slope.

The standardized CO_2 gas exchange velocities k_{600} (corresponding to a dimensionless Schmidt number of 600, valid at 20°C water temperature) were calculated from the two values of stream flow velocity v (equations (6) and (7)) and the channel slope S_{chan} using the equation from *Raymond et al.* [2012] (equation (8)). S_{chan} was estimated on the basis of a segmentation of the stream network according to the Strahler order [*Strahler*, 1952]. For each individual Strahler order segment, S_{chan} was calculated from the length of the segment and the decrease in its altitude extracted from the digital elevation models which are associated to the hydrological routing schemes. This procedure insured direct compatibility between the geometry of the stream network and altitude, which differs whether Hydro1k or Hydrosheds is used. The calculation of the catchment slope was performed using a different DEM (GLOBE DEM, 1 km resolution) because this geodata set has a global coverage and can thus be used to calculate slope gradients from differences in altitude between neighboring cells, at the same resolution everywhere within the domain, a prerequisite for a consistent assessment [*Jenson*, 1991; *Gessler et al.*, 2000]. The use of two different resolutions (Hydrosheds and Hydro1k) for the calculation of the average slope gradient of a stream segment is likely less problematic because these segments are generally several times longer than the cell lengths of the DEMs.

To calculate a gas exchange velocity representative of annual average conditions, we calculated monthly values of the actual gas exchange velocity k_{actual} from k_{600} and the estimated T_{water} [cf. *Raymond et al.*, 2012]. The monthly k_{actual} values were then averaged (discarding months with assumed ice cover or stream drying) to obtain the yearly value required for the calculation of FCO_2. The whole procedure was

performed once for the entire river network (i.e., for all streams with a minimum contributing area of 10 km^2) and once for two classes of streams and rivers, separately: (1) for streams and rivers with an average annual discharge $Q_{ann} < 100$ m^3 s^{-1} and (2) for rivers with $Q_{ann} \geq 100$ m^3 s^{-1}. The threshold Q_{ann} corresponds to a calculated stream width of 67–91 m (equations (4) and (5)). Thus, the two classes of streams and rivers reported here are comparable to those based on a threshold value for the width of 100 m [*Rasera et al.*, 2008, 2013; *Alin et al.*, 2011; *Aufdenkampe et al.*, 2011].

Our k values are comparable to those of *Raymond et al.* [2013] (supporting information). Our global A_{river} estimate of 291–415 × 10^3 km^2 is, however, significantly lower than the values reported in *Downing et al.* [2012] (485–662 × 10^3 km^2) and *Raymond et al.* [2013] (624 × 10^3 km^2). We consider the upper bound estimate by *Downing et al.* [2012] as best reference, because it is based on an extensive review of stream widths reported in the literature. Comparing our calculations to this reference, we conclude that we are missing the first two stream orders (see supporting information). As these smallest streams are also not represented in our pCO_2 database, our FCO_2 estimates only refer to stream orders 3 and higher. The first two stream orders represent only 11% of the total A_{river} in the estimate of *Downing et al.* [2012] and contribute only to a small part of his higher estimates. Moreover, we likely underestimate the width of stream orders 5 and higher (see supporting information). These larger rivers contribute over-proportionally to global A_{river} due to strong meandering and bifurcation into multiple reaches [*Downing et al.*, 2012], like, for instance, braided rivers in the high latitudes or the anastomosing lowland rivers in the humid tropics. Stream networks derived from DEMs as performed here do not account for stream channel bifurcations and inevitably lead to the underestimation of A_{river} for such systems [*Amos et al.*, 2008]. A likely better strategy is thus to use remote sensing or geodata to derive A_{river} for larger river systems [*Richey et al.*, 2002; *Striegl et al.*, 2012] and empirical GIS-based methods to estimate A_{river} for smaller streams [*Rasera et al.*, 2008, 2013; *Striegl et al.*, 2012; *Denfeld et al.*, 2013].

Following this approach, we recalculated a global value of A_{river} for $Q_{ann} > 100$ m^3 s^{-1}, using the river surface areas from the Global Lakes and Wetlands Database (GLWD) [*Lehner and Döll*, 2004]. GLWD reports only the large world rivers in vectorized format, the narrowest river stretches reaching several hundreds of meters of width, i.e., a value substantially wider than the minimum width in our estimates. In this alternative estimation of A_{river}, we calculated the GLWD river surface area for each 0.5° grid cell of our prediction grid. For each cell with a GLWD-derived river surface area higher than our estimate calculated above, we adopted the GLWD value. For the remaining cells, we kept our original estimates. In this way, we have a better representation of the largest rivers while still accounting for the smaller rivers not represented in GLWD.

With this method, we compute a global A_{river} of 699–832 × 10^3 km^2, which is now somewhat higher than the estimate by *Downing et al.* [2012]. However, our global $A_{river,eff}$ (510–596 × 10^3 km^2) is close to the estimate of *Raymond et al.* [2013] (536 × 10^3 km^2). The calculation of FCO_2 was updated by multiplying the average FCO_2 rate per river surface area by the revised values of $A_{river,eff}$. In what follows, we solely report the "GLWD-corrected" FCO_2 and A_{river} values.

2.3. Uncertainty Estimates Based on Monte Carlo Simulation

We calculated the expected values and uncertainty ranges (5% and 95% confidence interval) of pCO_2 and FCO_2 from a Monte Carlo simulation consisting of 10,000 runs. Gaussian error distribution was assumed for the coefficients (b estimates) of the four predictors of pCO_2, using the standard errors of the b estimates derived from the regression reported in Table 3. A uniform error distribution was imposed for k_{actual} and $A_{river,eff}$, over a range delimited by the two values calculated for each of these parameters using equations (4) and (5) and equations (6) and (7), respectively. We assume these errors to be uncorrelated to each other, i.e., the coefficients related to the predictors and the estimates of $A_{river,eff}$ and k_{actual} vary independently from each other. The Monte Carlo simulation was performed for each grid cell at the aggregated resolution of 0.5°. A similar approach, even with a reduced number of runs, would be computationally prohibitive at the higher resolution of the routing schemes.

For the Monte Carlo analysis performed at the aggregated 0.5° resolution, we ensured that the expected values for pCO_2 and FCO_2 were equal to the values calculated first at the high spatial resolution of the routing schemes and subsequently aggregated to the 0.5° resolution. To achieve this, we had to aggregate all the necessary input variables in a systematic way. The predicted pCO_2 was weighted by $A_{river,eff}$ (see section 2.1), using the average of the two calculated values of $A_{river,eff}$ (equations (4) and (5)). The values of

k_{actual} were weighted by $A_{river,eff}$, KCO_2, and pCO_2. To reproduce the half degree aggregation of estimated pCO_2 values weighted by $A_{river,eff}$, the first predictor was weighted by $A_{river,eff}$, the second predictor was weighted by the first predictor and $A_{river,eff}$, the third by the first two predictors and $A_{river,eff}$, and finally the fourth predictor was weighted by $A_{river,eff}$ and the other three predictors. All weightings and aggregations were performed in ArcGIS. After exporting the aggregated parameters as net-cdf files, the statistical language R 2.15.2 [*R Core Team*, 2013] including the "ncdf" package was used to run the Monte Carlo analysis. A comparison between the average values of pCO_2 and FCO_2 resulting from the 10,000 Monte Carlo runs and those calculated at the high resolution and then aggregated to 0.5° resolution revealed that for each half degree cell the relative deviation between the two approaches never exceeds 1%.

3. Results

3.1. Controls of Spatial Variation in pCO_2

We analyzed the correlation between the average pCO_2 of river water at the sampling location and 19 environmental variables attributed to the river catchment or the sampling location (Table 2). A notable positive correlation to pCO_2 was found for the catchment properties mean air temperature, precipitation, net primary production (NPP), and evaporation, while a strong negative correlation was found for the average slope gradient of the river catchment. Mean annual air temperature, annual precipitation, and evaporation at the sampling location show also notable positive correlations to pCO_2, while altitude and latitude of the sampling location are negatively correlated to pCO_2. The results for the slope gradient, mean air temperature, and precipitation are in accordance with the continental scale study for North America [*Lauerwald et al.*, 2013]. NPP and slope gradient were also shown to have an important influence on dissolved organic carbon in rivers [*Ludwig et al.*, 1996; *Lauerwald et al.*, 2012], which is partly decomposed during its fluvial transport and thus sustains the CO_2 oversaturation. A number of studies have suggested a downstream decrease in pCO_2 [*Finlay*, 2003; *Teodoru et al.*, 2009; *Aufdenkampe et al.*, 2011]. For our training catchments, however, the catchment area shows only a very low negative correlation to pCO_2 ($r = -0.06$) and the stream order (Strahler order) is not at all correlated to pCO_2. A low positive correlation ($r = 0.26$) was identified for population density, a result which might support an anthropogenic enhancement of river CO_2 evasion [*Kempe*, 1984; *Regnier et al.*, 2013]. Lakes and reservoirs are reported to decrease river pCO_2 due to increased residence times and autotrophic production [*Wang et al.*, 2007], but we found only a low negative correlation ($r = -0.16$) between this variable and pCO_2. The average flooded area around the sampling location (based on ~15 min cells, $r = 0.25$) or within the whole river catchment ($r = 0.22$) are, on the contrary, positively correlated to pCO_2. It is interesting to note that runoff shows no significant correlation to pCO_2, although precipitation and evaporation do.

Many of the environmental variables are highly spatially intercorrelated with one another (Table 2). Thus, a significant correlation between a variable and pCO_2 does not necessarily imply that this variable is a direct driver of the spatial variation in average pCO_2, and the effect might be more indirect (colinearity). The automated stepwise backward algorithm that we used for the multiple linear regression analysis is designed to select a set of robust predictors, the combination of which explains best the variance in the predicted variable ($log_{10}(pCO_2)$ in this case) and which avoids redundant predictor combinations. Based on the analysis, only four of the 19 parameters were retained as predictors: average slope gradient, annual NPP, population density within the river catchment, and mean annual air temperature at the sampling location. The equation combining these four predictors explains about 47% ($r^2 = 0.47$) of the spatial variation in $log_{10}(pCO_2)$ (Table 3). The model residuals show no significant correlation to any of the discarded parameters. The b estimates and the associated standard errors as well as the partial correlations of each retained predictor are listed in Table 3. Slope gradient shows the strongest partial correlation ($r = -0.53$) to $log_{10}(pCO_2)$, the other predictors showing all a positive partial correlation to $log_{10}(pCO_2)$ with an r of about 0.3. The coefficients attributed to the predictors (b estimates) can be interpreted in the following way: if two points in different river networks have identical predictor values, the regression equation predicts the same average pCO_2 for both. If for one of the two points the population density in the catchment is higher by 10 inhabitants per km^2, the predicted pCO_2 will be 7.1% higher than that for the other point, all other predictors being equal. Since in this case the predictor is the square root of population density, a positive difference of 100 inhabitants per km^2 would only yield an increase of
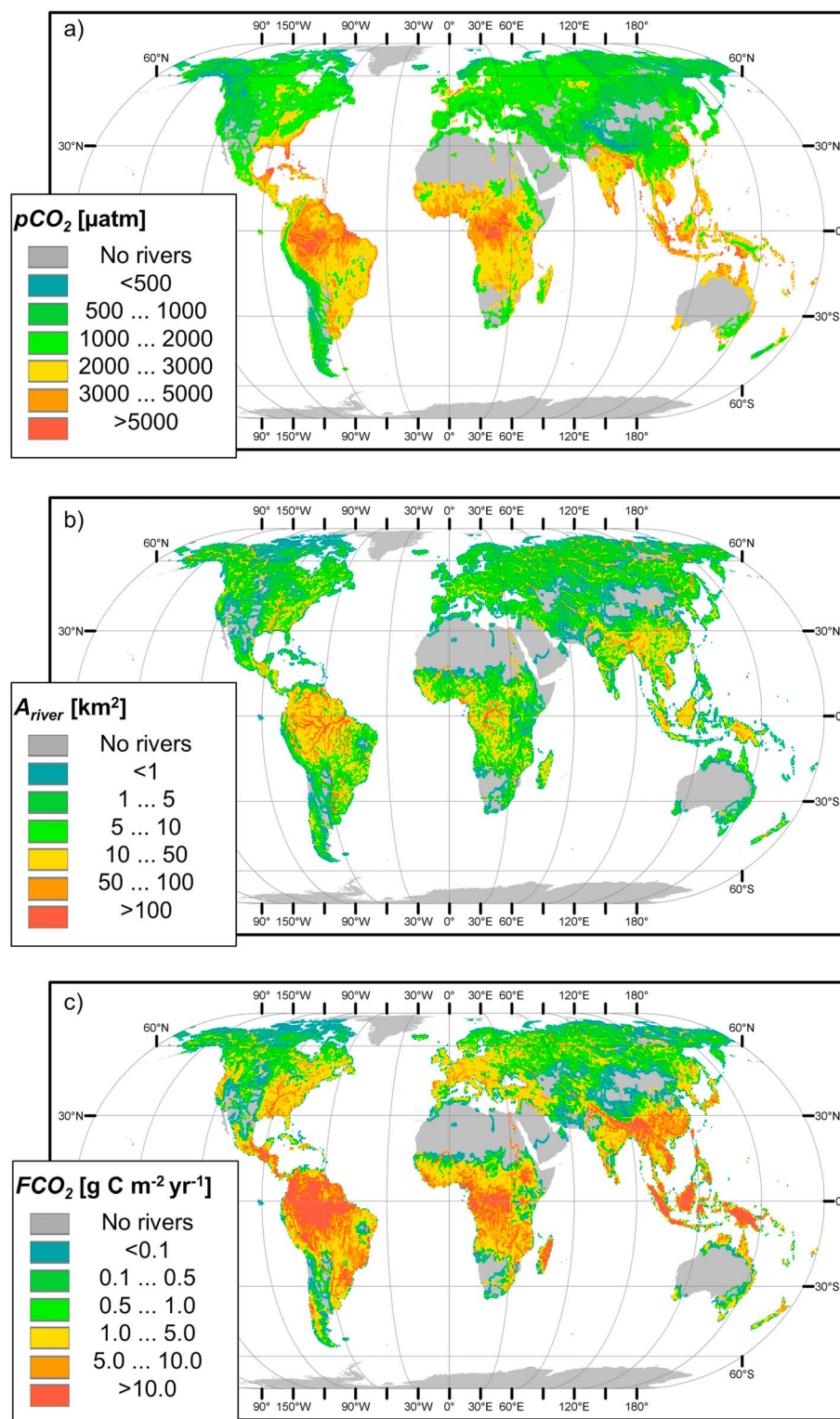
Figure 2. Predicted maps of (a) $p\text{CO}_2$, (b) A_{river}, and (c) $F\text{CO}_2$.

24.0% in predicted $p\text{CO}_2$. A positive difference in average NPP per catchment of 100 g C m^{-2} yr^{-1} or in mean air temperature of 2°C would translate into a predicted average $p\text{CO}_2$ that is 6.6% or 6.4% higher, respectively. The influence of average catchment slope gradient on $p\text{CO}_2$ is a bit more complicated to assess quantitatively, as this predictor is log transformed. For instance, an increase in average catchment slope
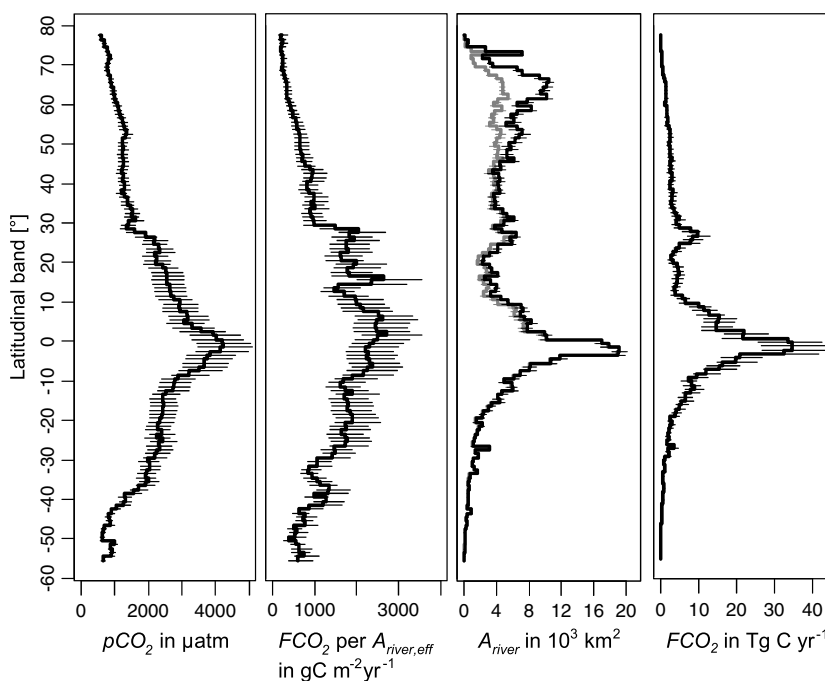
Figure 3. Latitudinal profiles of pCO_2, FCO_2 per $A_{river,eff}$, A_{river}, and total FCO_2. Values refer to 1° latitudinal bands. Thick lines represent the average estimates. Horizontal lines represent uncertainty range between the 5th and 95th percentiles, except for A_{river} where it represents the difference between values obtained from equations (4) and (5). The grey line in the plot for A_{river} represents the effective stream surface area $A_{river,eff}$.

gradient from 1° to 2° would result in a decrease in estimated pCO_2 of 18% while an increase from 5° to 6° would only lead to a decrease in estimated pCO_2 of 3%. Thus, by far, the most sensitive predictor is the catchment slope gradient, especially when the terrain is smooth. The larger sensitivity of pCO_2 to changes in gradient when the slope is small explains why very flat areas are generally characterized by high predicted pCO_2 values (see section 3.2).

3.2. Spatial Patterns of pCO_2, A_{river}, and FCO_2

The 0.5° map of pCO_2 (Figure 2a) shows increasing values from high to low latitudes, a global-scale spatial pattern that was already identified in previous studies [*Aufdenkampe et al.*, 2011; *Raymond et al.*, 2013] but without the high spatial resolution of this study. Most streams and rivers located between 30°N and 30°S exhibit a $pCO_2 > 2000$ μatm, with the exception of arid regions such as North Africa, the Arabic peninsula and central Australia, and the Western portion of the American continents. Predicted river pCO_2 values are generally higher in lowland areas than in steep mountain areas, in line with results from earlier regional scale studies [*Telmer and Veizer*, 1999; *Lauerwald et al.*, 2013]. Inland waters flowing through densely populated areas along the southern and eastern coasts of the U.S., the eastern coast of China, and the North Sea region, display pCO_2 values above 2000 μatm in spite of their relatively high latitudes and render the global spatial pattern more complex. The spatial distribution of river surface area A_{river} (Figure 2b) also reveals a well-established latitudinal gradient. Some of the largest rivers in the world, in particular, the Amazon, the Mississippi, the Congo, and the Ganges Rivers are clearly identifiable on the map by high A_{river} and FCO_2 values. The spatial distribution of FCO_2 per unit continental surface area further evidences the disproportionate contribution of equatorial and subtropical regions to the global riverine outgassing (Figure 2c). Most of the Amazon River basin, but also parts of the Congo River basin and SE Asia, outgas CO_2 at rates > 10 g C m^{-2} yr^{-1} (per total surface area, including the terrestrial domain).

The aggregation of our estimates per latitudinal bands of 1° shows that the average latitudinal pCO_2 varies by about 1 order of magnitude, with values ranging from below 600 μatm in high latitudes (>75°N) to more than 4000 μatm in low latitudes (between 1°N and 3°S, Figure 3). The spatial gradient of pCO_2 with latitude is not constant and pCO_2 remains below 2000 μatm north of 30°N and south of 40°S. The global average river pCO_2

Table 4. Comparison of Results to Previous Studies[a]

$p\text{CO}_2$ (µatm)	$F\text{CO}_2$ (Tg C yr^{-1})	$F\text{CO}_2$ (g C m^{-2} yr^{-1})	k (m d^{-1})	A_{river} (10^9 m^2)	Reference
		Global			
2400	650	1574	5.60–6.21	699–832	This study
(2019–2826)	(483–846)	(1238–1955)			
	230				*Cole et al.* [2007]
3100[b]	1800 ± 250				*Raymond et al.* [2013]
	560			310–510	*Aufdenkampe et al.* [2011]
		Global, Streams and Small Rivers			
2471	316	2004	6.61–8.64	142–255	This study
(2083–2906)	(214–438)	(1558–2513)			
	300			90–150	*Aufdenkampe et al.* [2011]
		Global, Large Rivers			
2299	334	1075	3.49–4.41	407–417	This study
(1933–2708)	(261–419)	(842–1344)			
	260			220–360	*Aufdenkampe et al.* [2011]
		Boreal-Arctic Zone (>50°), Streams and Small Rivers			
1152	14.4	543	4.00–5.26	34.9–64.1	This study
(1039–1274)	(9.73-19.9)	(434–663)			
1300	20	560	3.1	3–54	*Aufdenkampe et al.* [2011]
		Boreal-Arctic Zone (>50°), Large Rivers			
984	14.0	305	2.25–2.63	116–117	This study
(888–1086)	(11.4-16.8)	(251–364)			
1300	20	260	1.4	7–131	*Aufdenkampe et al.* [2011]
		Temperate Zone (25°–50°), Streams and Small Rivers			
1552	63.3	1351	7.58–10.2	39.5–71.2	This study
(1349–1772)	(42.7–88.2)	(1042–1701)			
3500	80	2630	4.8	29–34	*Aufdenkampe et al.* [2011]
		Temperate Zone (25°–50°), Large Rivers			
1368	48.7	648	3.95–5.32	82.2–84.8	This study
(1190–1562)	(37.3–61.7)	(526–862)			
3200	50	720	1.44	70–84	*Aufdenkampe et al.* [2011]
		Tropical Zone (<25°), Streams and Small Rivers			
3402	238	2829	6.90–8.86	68.0–120	This study
(2822–4054)	(162–330)	(2201–3551)			
4300	160	2720	4.1	60–60	*Aufdenkampe et al.* [2011]
3353 ± 2168		2065 ± 1285			*Alin et al.* [2011]
		Tropical Zone (<25°), Largel Rivers			
2974	271	1403	3.53–4.36	210–215	This study
(2471–3540)	(212–340)	(1099–1752)			
3600	230	1600	3	146–146	*Aufdenkampe et al.* [2011]
3317 ± 3089		1478 ± 1289			*Alin et al.* [2011]
		Yukon River System			
641	0.59	193	3.67–4.18	7.78–8.56	This study
(582–705)	(0.42–0.77)	(139–254)			
619-2690	7.68	750	3.1 (main)	10.3	*Striegl et al.* [2012]
			5.2 (trib)		
		Mississippi River System			
1708	9.14	758	2.96–3.20	13.1–16.3	This study
(1484–1918)	(7.18–11.3)	(632–897)			
1335 ± 129	13	1182 ± 390		8.5	*Dubois et al.* [2010]
		Central Amazon Basin, Quadrant 0°N, 72°W to 8°S, 54°W			
4453	83.7	2035	3.40–3.47	47.1–50.8	This study, w. GLWD
(3666–5338)	(65.3–105)	(1629–2491)			
	290			143	This study, using avg. inundation
	(232–355)				area from *Prigent et al.* [2007]
4350 ± 1900[c]	210 ± 60	830 ± 240		79–290[d]	*Richey et al.* [2002]
5000 ± 3300[e]					

Table 4. (continued)

$p\mathrm{CO_2}$ (µatm)	$F\mathrm{CO_2}$ (Tg C yr^{-1})	$F\mathrm{CO_2}$ (g C m^{-2} yr^{-1})	k (m d^{-1})	A_{river} (10^9 m^2)	Reference
	360 ± 65	1880 ± 340			*Rasera et al.* [2013]
		Ji-Parana River Basin			
3195	1.00	1849	3.38–4.74	0.53–0.69	This study
(2698–3751)	(0.76–1.28)	(1498–2246)			
	0.31 ± 0.19			0.31–0.37[f]	*Rasera et al.* [2008]
		Ji-Parana River Basin, Small Streams and River			
3431	0.55	2215	4.36–5.27	0.18–0.31	This study
(2894–4030)	(0.38–0.74)	(1789–2696)			
		2079 ± 1197		0.15–0.19[f]	*Rasera et al.* [2008]
		Amazon Basin, Stream and Small Rivers			
	51			13.1–22.7	This study
	(35.4–69.7)				
	170 ± 42			300 ± 50	*Rasera et al.* [2008]
		Amazon River System			
3929	159	1946	4.23–4.27	92.6–103	This study
(3228–4726)	(123–201)	(1567–2412)			
	476			244	This study, using average inundation area from *Prigent et al.* [2007]
	(383–590)				
	470				*Richey et al.* [2002]
	800				*Rasera et al.* [2013]
		Sweden			
995	0.37	459	3.33–3.96	0.98–1.49	This study
(900–1097)	(0.27–0.49)	(374–553)			
1,349	0.85	473–3032[g]	6–15	0.5	*Humborg al.* [2010]
		Conterminous USA			
1690	18.6	831		24.9–32.1	This study
(1484–1918)	(14.2–23.7)	(681–999)			
	96.8	2370 ± 800		40.6	*Butman and Raymond* [2011]

[a]Streams and small rivers are defined by stream width smaller than 60–100 m for the values of *Aufdenkampe et al.* [2011], by a stream width smaller than 100 m by *Alin et al.* [2011] and *Rasera et al.* [2008], and by an annual discharge $Q_{\mathrm{ann}} < 100\ \mathrm{m^3\ s^{-1}}$ in our study (which gives a stream width of 67–91 m according to the equation by *Raymond et al.* [2013] and *Raymond et al.* [2012], respectively). $F\mathrm{CO_2}$ in g C m^{-2} yr^{-1} refers to effective stream surface area $A_{\mathrm{river,eff}}$. With the exception of *Striegl et al.* [2012], all literature values of k refer to k_{600} (i.e., normalized to 20°C water temperature).
[b]Based on spatial interpolation and normalized by stream surface area.
[c]Refers to Amazon main stem in the central Amazonian Basin.
[d]Area of the main stem and tributaries including their floodplains; the given range is the seasonal change in surface water area.
[e]Refers to the mouth of the major tributaries of the Amazon river.
[f]Lower values represent mean estimate for low water stages, higher values the mean estimate for high water stages.
[g]Highest value for stream order 1 and lowest value for stream order 6.

is 2400 µatm, with a 2019–2826 µatm uncertainty range based on the 5th and 95th quantiles. $F\mathrm{CO_2}$ per unit surface water area shows a latitudinal trend similar to that of $p\mathrm{CO_2}$, with average values < 500 g C m^{-2} yr^{-1} above 55°N, and > 2000 g C m^{-2} yr^{-1} below 10° (Figure 3). The latitudinal distribution of the stream surface area A_{river} allows to identify a narrow maximum ($>16,000$ km^2 per 1°) around the equator corresponding to the Amazon and Congo river main stems (Figures 2 and 3). A second maximum of A_{river} occurs in the high northern latitudes ($>50°$N). Due to the increased importance of cold seasons, $A_{\mathrm{river,eff}}$ is nevertheless rather monotonously distributed over the Northern middle to high latitudes. The relatively low values around 15°N originate from the abundance of arid areas (e.g., Sahara) in these regions. Overall, of an estimated global average A_{river} comprised between 699–832×10^3 km^2 (based on equations (4) and (5), respectively), the 10°N–10°S latitudinal band contributes about one fourth (181–211×10^3 km^2).

Globally, the total $F\mathrm{CO_2}$ is estimated at 650 Tg C yr^{-1}, with an uncertainty range of 483 to 846 Tg C yr^{-1} (5th and 95th percentiles from the 10,000 Monte Carlo simulations). The spatial pattern of $F\mathrm{CO_2}$ is a logical product of the distribution of A_{river} and $F\mathrm{CO_2}$ per unit stream surface area, leading to an even more pronounced latitudinal gradient (Figure 3). The zonal band comprised between 10°N and 10°S exhibits a total $F\mathrm{CO_2}$ of

371 (279–479) Tg C yr^{-1} and thus contributes more than half of the global CO_2 evasion flux. A smaller, secondary peak that corresponds to the contribution of the Ganges and several Chinese rivers is observed between 25°N and 30°N. For latitudes higher than 50°, we estimate a total FCO_2 of only 28.4 (21.4–36.3) Tg C yr^{-1}, less than 5% of the global CO_2 evasion.

A_{river} of streams and small rivers with $Q_{ann} < 100$ m^3 s^{-1} calculated with equation (5) or (4), contribute 20% or 31% of the total surface area (Table 4), respectively. The gas exchange velocity k_{actual}, which averages to 6.61–8.64 m d^{-1} in streams and rivers with $Q_{ann} < 100$ m3 s^{-1} and 4.41–3.49 m d^{-1} in rivers with higher Q_{ann}, favors a more intense outgassing from smaller streams and rivers. The estimated average CO_2 evasion rate per stream surface area for this class of rivers is 2004 (1558–2513) g C m^{-2} yr^{-1}, a value which is nearly twice that estimated for rivers with $Q_{ann} > 100$ m3 s^{-1}, 1075 (842–1344) g C m^{-2} yr^{-1}. Thus, despite their relatively low contribution to A_{river}, small stream and rivers contribute about half of the global FCO_2 calculated here.

4. Discussion

4.1. Comparison to Previous Studies

Our estimated global FCO_2 of 650 (483–846) Tg C yr^{-1} is significantly higher than that of 270 Tg C yr^{-1} by *Cole et al.* [2007], slightly, but not significantly higher than that of 560 Tg C yr^{-1} by *Aufdenkampe et al.* [2011] but nearly three times lower than the most recent estimate of 1800 Tg C yr^{-1} by *Raymond et al.* [2013] (Table 4). The estimate by *Cole et al.* [2007] only refers to large rivers, and taking into account that streams and small rivers are also an important net source of CO_2 to the atmosphere (Table 4), it is not surprising that our global outgassing is significantly higher. Note that all global estimates, including the present study, ignore the first-order streams. *Raymond et al.* [2013] attempted a very first quantification by extrapolating their results for A_{river} and k in stream orders 3 to 5 to stream order 1. However, such approach does not account for increased pCO_2 in first-order streams fueled by inputs of fresh soil/ground water. The contribution of headwaters to the global fluvial FCO_2 is thus not yet constrained.

The FCO_2 per latitudinal zone are quite similar to those reported by *Aufdenkampe et al.* [2011] (Table 4), with the exception of FCO_2 from tropical streams and smaller rivers which is significantly higher here (238 (162–330) Tg C yr^{-1} versus 160 Tg C yr^{-1}). Our global spatial pattern of river pCO_2 and FCO_2 is also in qualitative agreement with the one reported in *Raymond et al.* [2013]. Our global quantification of FCO_2 is lower mainly due to more conservative estimates of river pCO_2, particularly in the tropics. While the highest pCO_2 averaged over an entire COSCAT is estimated here at 3823 (3163–4564) μatm (COSCAT #1104, Amazon Basin), the maximum median pCO_2 value per COSCAT reaches 11,772 μatm in *Raymond et al.* [2013].

Due to methodological limitations and the coarse resolution of the DEMs used, our analysis likely misses up to two stream orders [*Benstead and Leigh*, 2012]. Ten stream orders are accounted for in our study, while *Downing et al.* [2012] accounted for 12 stream orders in their analysis. This supports the idea of a river pCO_2 and FCO_2 estimation for stream orders 3 and higher only, which excludes smaller headwater streams. Applying scaling laws on the total stream length and average stream width (see supporting information), we estimate A_{river} for the lowest two stream orders at ∼ 40 × 10^3 km^2 each. Together, they would thus contribute to about 10% of the global A_{river} estimated here, a proportion quite close to that estimated by *Downing et al.* [2012] (11%). The contribution of stream orders 1 and 2 to FCO_2 is, however, likely higher because of their high CO_2 supersaturation and high gas exchange velocities. For headwater streams in tropical uplands, for instance, average pCO_2 values as high as 19,000 μatm [*Davidson et al.*, 2010] and even 50,000 μatm [*Johnson et al.*, 2008] have been reported. The major part of this CO_2 already evades within the first-order streams [*Johnson et al.*, 2008]. A similar behavior has been observed in small, peat-covered catchments in Scotland [*Dawson et al.*, 2001; *Dinsmore et al.*, 2013] and the subarctic [*Denfeld et al.*, 2013; *Lundin et al.*, 2013]. The high CO_2 oversaturation from headwaters is mainly fed by soil and plant root respiration which evade not far downstream from their source [*Davidson et al.*, 2010]. Farther downstream, fresh soil water inputs are less important, and CO_2 oversaturation is mainly maintained by instream respiration of organic matter [*Park et al.*, 1969; *Kempe*, 1984; *Ward et al.*, 2013]. Riverine wetlands can also be important sources of labile organic carbon and direct CO_2 inputs from autotrophic respiration sustained by submerged parts of floodplain vegetation, particularly in tropical lowland rivers [*Richey et al.*, 2002; *Mayorga et al.*, 2005; *Abril et al.*, 2014].

Existing regional and global estimates do not always address all compartments of the inland water network, and the distinction between semiaquatic and aquatic systems is rarely performed in a systematic way. In addition, major differences in methodological approaches make direct comparison between estimates difficult. For the tropics, the Amazonian Basin is the best surveyed area and several published studies are available for comparison. For the basin of the Ji-Parana River, a tributary of the Rio Madeira in SW Amazonia without major influence of floodplains, *Rasera et al.* [2008] investigated aquatic CO_2 evasion, with a focus on small rivers with widths < 100 m, yet which excludes contributions from headwater streams (Table 4). While our estimate of CO_2 evasion rate per surface water area of these small rivers is quite similar to their values, our estimate of A_{river} is about 50% higher.

For the Central Amazon basin, defined by the quadrant between 0°N, 72°W and 8°S, 54°W, the hydrology and river biogeochemistry are strongly influenced by floodplain dynamics [*Hess et al.*, 2003; *Melack et al.*, 2009]. The total CO_2 evasion increases with flooded area and is highest in May when about 20% of the quadrant is flooded [*Richey et al.*, 2002]. Our average estimate of riverine pCO_2 of 4453 (3666–5338) μatm for this area matches closely the 4350 ± 1900 μatm reported by *Richey et al.* [2002], and the average CO_2 evasion rates per surface water area reported here are not significantly different from that of *Rasera et al.* [2013]. In our calculation, however, floodplains are not included in A_{river} and thus our total FCO_2 for this quadrant is substantially lower than those from the literature which include floodplains (Table 4). If we use the average flooded area from the data set of *Prigent et al.* [2007] (143×10^3 km^2) to account for the total surface area of rivers and floodplains and multiply it by our estimated average CO_2 evasion rates (per surface area), we obtain an FCO_2 of 290 (232–355) Tg C yr^{-1} which falls between the 210 ± 60 Tg C yr^{-1} by *Richey et al.* [2002] and the 360 ± 65 Tg C yr^{-1} by *Rasera et al.* [2013]. For the tropical zone ($<25°$) in general, our estimated averages of river pCO_2 and CO_2 evasion rates per surface area are not significantly different from those reported by *Alin et al.* [2011]. Although our study focuses on the river network only and ignores the contribution of floodplains to the total water-air gas exchange, our estimates are quite well in accordance with other regional studies. Extrapolating their results to the whole Amazon Basin, *Richey et al.* [2002] estimate the FCO_2 to 470 Tg C yr^{-1} and *Rasera et al.* [2013] to 800 Tg C yr^{-1}, from which a considerable part is attributed to the evasion from floodplains. For streams and rivers excluding floodplains we estimate the FCO_2 to 159 (123–201) Tg C yr^{-1}. According to *Johnson et al.* [2008], FCO_2 from upland first-order streams ignored in our calculation could add another 114 ± 10 Tg C yr^{-1}.

Our estimate of average pCO_2 in Swedish rivers is about 40% lower than that reported by *Humborg et al.* [2010]. At first glance, this may appear surprising since the database for Swedish rivers was included in the training data for our statistics. However, only a subset was used, because it was not possible to extract the catchment properties corresponding to all sampling locations with the required quality. This mainly applies to the small catchments corresponding to headwater streams, which could not be resolved in a suitable way at the spatial resolution of the routing schemes, and the flat areas where the low gradients in altitude prevented accurate reconstruction of the watershed boundaries. Taking into account that both flat areas (see section 3.1) and small headwater streams tend to show comparatively high pCO_2 [*Humborg et al.*, 2010; *Wallin et al.*, 2013], the difficulty to delineate small and very flat river catchments might have introduced a bias in our training data for pCO_2. Likely for similar reasons, our average estimate of pCO_2 for the Yukon River basin is at the lower end of the observed values reported by *Striegl et al.* [2012]. In addition, our comparatively low estimates of FCO_2 can also result from the likely omission of the first two stream orders, which are better accounted for in regional studies. The estimate of *Humborg et al.* [2010] extrapolated to the total land surface area of Sweden would translate into an FCO_2 of around 2 g C m^{2}yr^{-1}, about twice our estimate. The area specific FCO_2 for the Yukon is estimated at 9 g C m^{-2}yr^{-1} [*Striegl et al.*, 2012], which is close to 10 times higher than our estimate. Similar area specific FCO_2 (5–9 g C m^{-2}yr^{-1}) were reported for a 15 km^2 subarctic headwater catchment in Northern Sweden [*Lundin et al.*, 2013] and for a 67 km^2 boreal catchment in Sweden [*Wallin et al.*, 2013]. Again, these high values could reflect the significant contribution of the smallest streams which we miss in our study. In particular, high FCO_2 rates were reported for headwater catchments where wetlands are abundant. For instance, two small Scottish upland catchments (<5 km^2) with peat cover exhibit FCO_2 values as high as 10–14.1 g C m^{-2}yr^{-1} [*Hope et al.*, 2001; *Dinsmore et al.*, 2013]. Peatlands are, however, environments with particularly high CO_2 evasion from headwater streams [*Worrall et al.*, 2009; *Rawlins et al.*, 2014]. Over the entire area of England

and Wales, *Rawlins et al.* [2014] estimate the CO_2 evasion from headwater streams at 0.44 g C m^{-2} yr^{-1} only, i.e., more than 1 order of magnitude lower than the values reported for the two peat-covered catchments in Scotland. Compared to our FCO_2 estimates (stream order 3 and higher) of 1–5 g C m^{-2} yr^{-1} for the British Islands (Figure 2), this would still represent a significant contribution of smallest streams to the FCO_2 from the river network missed by our approach. Areas with extensive peat cover, particularly in permafrost regions, could nevertheless contribute to high FCO_2 over significant portions of the land in high latitudes. In our statistical model, the effects of peatlands and permafrost are not represented, which might be another reason for underestimating pCO_2 and, thus, FCO_2 in the Yukon River basin.

In temperate North America, we can compare our results to two regional studies. *Dubois et al.* [2010] used stable carbon and oxygen isotopes to assess carbon cycling in the Mississippi river and the resulting CO_2 evasion rate per unit water surface area is about 50% higher than the value reported here, albeit our average river pCO_2 is larger (Table 4). Overall, our estimates of A_{river} and FCO_2 are 73 ± 19% higher and 30 ± 16% lower, respectively. Compared to the study by *Butman and Raymond* [2011] for the conterminous U.S., our estimated average CO_2 evasion rate per unit water surface area is 65% lower while the value of A_{river} is 32 ± 7% lower (Table 4). The average pCO_2 per stream order ranges from about 3000 µatm for first-order streams to about 2000 µatm for stream order 9, while our overall average estimate of pCO_2 is lower with 1690 (1484–1918) µatm. As in our study, the U.S. is quite well covered with training catchments ($N = 498$), it can be assumed that our prediction function does not show a specific bias for that area. The arithmetic mean of our calculated pCO_2 per sampling location for the U.S. (1807 ± 1599) is indeed not significantly different from our spatially explicit estimate. The different estimates of pCO_2 and FCO_2 are thus partly due to differences in provenance and treatment of river chemistry data.

4.2. Upscaling and Methodological Limitations
4.2.1. Upscaling Techniques

Regionalized estimates of FCO_2 require an a priori delineation of regions for which representative values of A_{river}, k, and pCO_2 can be obtained. *Aufdenkampe et al.* [2011] established estimates for three latitudinal zones distinguishing the contribution of streams and smaller rivers (up to 60 to 100 m wide) on the one hand and larger rivers on the other hand. *Raymond et al.* [2013] went a step farther and used 231 COSCAT segments to regionalize their global estimate. These COSCAT regions comprise multiple river basins and were originally designed to quantify land to ocean matter fluxes [*Meybeck et al.*, 2006; *Laruelle et al.*, 2013] rather than the vertical exchange of CO_2 between inland water bodies and the atmosphere. Average values of A_{river} and k per stream order within each COSCAT were estimated, while only one average pCO_2 value for the whole river network belonging to a particular COSCAT segment was calculated. In their study focusing on the inland waters of Sweden, *Humborg et al.* [2010] constructed a stream network from a DEM and estimated averages of stream width B, k, and pCO_2 per stream order to calculate FCO_2. Here instead of regionalized lumped estimates, we developed an empirical prediction framework that allows for the first time estimates of A_{river}, k, pCO_2, and FCO_2 along a grid at a 0.5° resolution. This approach does not only provide values for individual river system but resolves also the variations along a given river system. In particular, instead of using regionalized averages and a segmentation of the river network into stream orders for the calculation of pCO_2, we first analyzed the correlations between environmental variables and the average pCO_2 per sampling location and derived a statistical model which we then used to predict a continuous, spatial representation.

It is, however, important to note that the heterogeneous spatial coverage of the training data may induce biases in our calculations. The statistical model can be used to extrapolate estimates of pCO_2 and FCO_2 from areas with good data coverage to areas with coarse data coverage if they are similar with regard to the identified environmental drivers. Although the broad variety of climatic zones is covered in our analysis, the tropical zone and the high latitudes are underrepresented in the training data set, while the more populated areas in North America, Europe, and Australia contribute disproportionally to the data. For the Amazon, our estimates are in good agreement with observed values from the literature. In the future, new regional studies will show if our estimates are also valid for tropical Africa and Asia. Our empirical model tends to underestimate pCO_2 and FCO_2 from boreal rivers reported in several regional studies. Our pCO_2 estimates are nevertheless coarsely in agreement with the average pCO_2 calculated at each sampling location in these areas (supporting information, Figure S3), and this might indicate that the sampling

locations retained for our statistical analysis are not sufficiently representative of these regions, partly due to the difficulty to derive catchment boundaries based on a DEM in flat areas.

Much alike other regional and global-scale studies [*Humborg et al.*, 2010; *Butman and Raymond*, 2011; *Lauerwald et al.*, 2013; *Raymond et al.*, 2013; *Laruelle et al.*, 2015], we calculated pCO_2 from alkalinity, pH, and water temperature, which is associated to considerable uncertainties. A difference in pH of 0.1 units leads to a change in pCO_2 of about 20% [*Lauerwald et al.*, 2013]. By first calculating monthly median values from at least three single values, we attempted to minimize the errors introduced by the pCO_2 calculation method. Furthermore, all samples with a pH lower than 5.4 were discarded, because for such low pH values calculation of pCO_2 becomes too uncertain [*Raymond et al.*, 2013], mainly because of noncarbonate contribution to titrable alkalinity [*Hunt et al.*, 2011]. The exclusion of low-pH rivers might have introduced some bias, because those conditions are typical of, e.g., black water rivers draining ombrotrophic wetlands. According to *Wallin et al.* [2014], the difficulty to calculate pCO_2 for rivers with very low alkalinity affects particularly boreal headwater streams. These water bodies can be an important source of CO_2 to the atmosphere and could be overlooked in our study or in *Raymond et al.* [2013]. This potential bias may also affect the representativeness of our training data, and our pCO_2 estimates could thus be too low in boreal regions. Due to the underrepresentation of such specific environments in the training data set, it is likely that potentially important drivers of river pCO_2, e.g., flat areas in high latitudes (peatlands) and low-pH blackwater streams, have been missed in our statistical analysis (see section 4.2.2). To overcome these limitations, more systematic, direct observations of river pCO_2 and better-suited hydrological routing schemes for high-latitude systems will be needed.

4.2.2. Selection of Predictors

As a result of the resolution of the hydrological routing schemes, our pCO_2 prediction model misses the first two stream orders and the smallest headwater catchments are not represented in our database (95% of the 1182 training catchments are larger than $48\ km^2$). Because Hydro1k is coarser and of lower quality than Hydrosheds, a precise delineation of watersheds is harder to achieve at high latitudes, in particular, for small catchments and in flat areas. Thus, the bias introduced by omitting small catchments might be the strongest in boreal to arctic latitudes and likely contributes to the underestimation of pCO_2 in these areas.

If we assume that most of the downstream decrease in pCO_2 occurs over the first two stream orders, as suggested in the literature (see preceding section), the lack of headwater catchments in our training data might explain why the correlation between catchment size and river pCO_2 ($r = -0.06$) is so low. In their study on North American rivers using a similar method, *Lauerwald et al.* [2013] also found no effects of catchment size on pCO_2 or on the relationship between pCO_2 and other environmental variables. Nevertheless, we estimate on average higher pCO_2 values for stream and smaller rivers ($Q_{ann} < 100\ m^3\ s^{-1}$) than for larger rivers (Table 4).

Within larger rivers, pCO_2 does not necessarily decrease downstream, for instance, because fresh inputs of CO_2 and labile organic carbon from floodplains maintain high levels throughout [*Mayorga et al.*, 2005; *Wang et al.*, 2013; *Abril et al.*, 2014]. The low positive correlation between percentage of inundated area and pCO_2 ($r = 0.25$) is consistent with this finding. Yet it was not retained as predictor because this parameter shows a strong intercorrelation with the average slope gradient within the catchment, the most sensitive predictor for the river pCO_2. Average catchment slope gradient was already identified as the main predictor for fluvial dissolved organic carbon exports, while areal proportion of wetlands was of lower importance to describe spatial variations [*Lauerwald et al.*, 2012]. A larger number of observed pCO_2 covering interconnected fluvial-wetland systems in low- and high-latitude regions might help better constrain the effects of wetlands on pCO_2 in the future.

Downstream increases in pCO_2 can also occur when rivers flow through more densely populated areas where anthropogenic point sources of labile organic carbon feed instream respiration [*Kempe*, 1984; *Garcia-Esteves et al.*, 2007; *Vanderborght et al.*, 2007]. We retained population density within the catchment as predictor, which can be regarded as proxy for anthropogenic inputs of organic C. Those inputs depend, however, on the quality of waste water treatment and on agricultural practices. With the majority of training data being distributed over North America and Europe, the relationship between population density and river pCO_2 found here is not necessarily valid for Asia and Africa. Taking into account that we removed data from the high-pollution period in Europe, i.e., before 1990 [cf. *Amann et al.*, 2012], we might underestimate river pCO_2 in populated catchments located in less-developed countries. The only retained predictor directly related to

climate is mean air temperature. It is likely the most important climatic variable, as respiration rates in soil and the water column increase with temperature. The fourth predictor, average NPP, is also strongly correlated with air temperature ($r = 0.45$), precipitation ($r = 0.62$), and evaporation ($r = 0.61$) and is a good measure of the potential C exports to rivers.

4.2.3. Stream Surface Area A_{river}

The estimation of A_{river} from stream networks derived from DEMs, as performed here and in other studies [*Humborg et al.*, 2010; *Butman and Raymond*, 2011; *Raymond et al.*, 2013], is subject to several technical limitations. First, the first two stream orders cannot be properly captured due to the coarse resolution of global DEMs. This problem can partly be overcome by using DEMs with higher resolutions, which are so far only available for regional scale studies [*Humborg et al.*, 2010; *Butman and Raymond*, 2011]. Second, the networks derived from DEMs do not account for bifurcations in downstream direction. Thus, for large river systems with complex geometries, particularly anastomising tropical lowland rivers as well as braided rivers in high latitudes, A_{river} is underestimated. A direct comparison of average stream width per stream order with those of *Downing et al.* [2012] which do account for bifurcations clearly reveals that our uncorrected results and those of *Raymond et al.* [2013] underestimate the stream width of such rivers (see supporting information). So far, the best practice to assess A_{river} in a spatially explicit manner is to use remote sensing (or geodata derived from these products) to calculate the surface area of large rivers and high-resolution DEM to estimate the surface area of smaller headwater streams, as already performed in regional studies [*Striegl et al.*, 2012; *Denfeld et al.*, 2013]. This approach was followed here and we corrected our estimates for the large rivers using the river surface data from GLWD [*Lehner and Döll*, 2004].

While many rivers with a confined stream channel exhibit widths that do not change much unless very large floods occur, several major river systems, for instance, the central Amazon basin, periodically inundate large floodplains. In the Amazon, a remote-sensing campaign was carried out to assess the seasonal changes in inundated areas [*Hess et al.*, 2003] and various studies on water-air CO_2 exchange have since then profited from this effort [*Richey et al.*, 2002; *Rasera et al.*, 2013; *Abril et al.*, 2014]. In our global study, we did not include the floodplains as an integral part of the river system. The global data set from *Prigent et al.* [2007] is based on spaceborne remote-sensing data that only detect extensive inundated areas and thus tend to underestimate their global significance. Technical progress in this area will certainly facilitate the analysis of carbon and CO_2 floodplain dynamics and its impact on the global river network.

4.2.4. Gas Exchange Velocity k

The estimation of the gas exchange velocities represents another considerable source of uncertainty. It is based on empirical equations derived from a restricted number of training sites and specific flow/weather conditions. As a result, different empirical equations have been proposed, which lead to distinct quantitative estimations. For smaller streams, the dominant controlling factors of k are discharge, stream flow velocity, depth and width of the channel, and stream bed roughness [*O'Connor and Dobbins*, 1958; *Owens et al.*, 1964; *Melching and Flores*, 1999; *Wallin et al.*, 2011; *Raymond et al.*, 2012]. For larger rivers, k may be controlled by stream flow currents and wind effects [*Vanderborght et al.*, 2002; *Borges et al.*, 2004; *Alin et al.*, 2011], the latter depending on wind speed, length of open water surface in the wind direction, surrounding topography, and vegetation. The empirical equations established in the studies referenced above are generally reduced to a few of these controlling factors, albeit other factors still do have an influence. Therefore, applying these empirical equations to systems that are fundamentally different from the training set can lead to erroneous estimates.

In our study, we used stream channel slope and discharge as ultimate predictors for k (equations (6)–(8)) [*Raymond et al.*, 2012, 2013]. The prediction equation was derived from 563 direct gas tracer release experiments throughout the U.S. [*Raymond et al.*, 2012]. For the hydraulic equations required to estimate stream width, depth, and velocity from discharge, additional observations from 9811 gauging stations were used [*Raymond et al.*, 2013]. Compared to other empirical equations published in the literature, this is by far the largest training data set and it covers a wide range of discharge and environmental conditions. *Raymond et al.* [2013] calculated the average stream channel slope for the stream orders 2–4 per COSCAT and then used scaling laws to estimate the channel slopes of the other stream orders. Here we calculated the channel slope for each individual stream segment separately. Aggregating our individual estimates to global averages per stream order, we nevertheless obtain results which support the validity of scaling laws for stream orders 2–6. Only for the smallest streams belonging to stream order 1 (which would be a stream order 3, because we miss two stream orders), the channel slope is slightly underestimated (7%, see supporting information).

The estimated k values derived here are also comparable to observed k values in the Yukon River system (Table 4). In addition, our FCO_2 rates from tropical rivers across a wide range of sizes are similar to observed average values and our estimates of k are thus likely reasonable. Some large, low-gradient river systems under strong influence from the wind might reveal higher k values than calculated here [cf. *Beaulieu et al.*, 2012]. This might explain why our FCO_2 for the Mississippi river system is lower than previously reported [*Dubois et al.*, 2010].

While the predictive equations used here only allow for the calculation of annual averages, gas exchange velocities vary considerably in time as a response to changes in discharge and wind speeds [*Alin et al.*, 2011; *Wallin et al.*, 2011]. Yet k has also an effect on the temporal variations of pCO_2. The combination of instantaneous pCO_2 and k measurements would help to decrease the uncertainty of calculated FCO_2. This is an important argument for the use of direct observation of FCO_2 rates per stream surface area for upscaling, which will, however, require more systematic field work and the assembly of a global database.

5. Conclusion and Outlook

We developed a statistical model which predicts the global spatial patterns in average river water pCO_2 ($r^2 = 0.47$). A total of 1182 training catchments were used for the statistics, and the selected predictors are average slope gradient, mean air temperature, NPP, and population density. A notable correlation between river pCO_2 and precipitation or evaporation was also found, but these climate variables are redundant predictors as they show strong correlations to NPP. The identification of population density as a controlling factor of river pCO_2 indicates a direct anthropogenic effect on greenhouse gas dynamics likely related to point source injection of labile organic carbon. According to various projections [*Friend et al.*, 2014], population density, air temperature, and NPP will increase in most regions of the globe. Since river pCO_2 is positively correlated to these three predictors, an increase in river pCO_2 can be expected in the coming decades.

We calculated a global FCO_2 of 650 (483–846) Tg C yr^{-1}. This estimate is likely conservative because our calculations ignore the first two stream orders which are expected to contribute significantly to FCO_2 due to inputs of CO_2 from soil respiration. The FCO_2 from small headwater streams has not yet been constrained at the global scale and remains a research challenge for the years to come. With this study, we went beyond regionalized lumped estimate of global FCO_2 and proposed the first continuous representations of pCO_2 and FCO_2 on a grid at 0.5° resolution. The resulting products are better suited to resolve spatial patterns, because instead of imposing a priori delineations between regions, they directly emerge from the statistically derived environmental drivers that are included in our prediction. The results highlight the importance of tropical rivers in the global picture of CO_2 evasion. Our estimates for the Amazon, which is the best-monitored tropical river basin, compares well with regional studies. For high latitudes, our statistical model tends to underestimate river pCO_2 and thus FCO_2, partly due to a skewed pCO_2 database which lacks smaller catchments in these areas. A larger set of data with more catchments, particularly of smaller size, could help in identifying additional controlling factors. Although empirical statistical modeling coupled to GIS integration offers promising avenues to fill gaps in spatial coverage, additional observations, in particular, direct observations of pCO_2 and FCO_2 rates in hotspot areas such as Siberia and tropical Africa and Asia are still needed to further improve the present budget. In the future, mechanistic modeling approaches, starting from the upland soils and including riparian wetlands and lakes, will help improve our understanding of the spatial and temporal dynamics of carbon fluxes through the global fluvial network and identify the climatic and anthropogenic drivers of these fluxes [*Regnier et al.*, 2013]. In the long run, combined observational modeling efforts will support future projections of global CO_2 evasion from the river network. In this context, the integration of carbon fluxes through inland waters into Earth System models is needed to improve the carbon budgets of the continents.

References

Abril, G., et al. (2014), Amazon River carbon dioxide outgassing fuelled by wetlands, *Nature*, *505*(7483), 395–398, doi:10.1038/nature12797.

Alin, S. R., M. D. F. F. L. Rasera, C. I. Salimon, J. E. Richey, G. W. Holtgrieve, A. V. Krusche, and A. Snidvongs (2011), Physical controls on carbon dioxide transfer velocity and flux in low-gradient river systems and implications for regional carbon budgets, *J. Geophys. Res.*, *116*, G01009, doi:10.1029/2010JG001398.

Amann, T., A. Weiss, and J. Hartmann (2012), Carbon dynamics in the freshwater part of the Elbe estuary, Germany: Implications of improving water quality, *Estuarine Coastal Shelf Sci.*, *107*, doi:10.1016/j.ecss.2012.05.012.

Amos, K. J., J. C. Croke, A. O. Hughes, J. Chapman, I. Takken, and L. Lymburner (2008), A catchment-scale assessment of anabranching in the 143 000 km^2 Fitzroy River catchment, north-eastern Australia, *Earth Surf. Processes Landforms*, *33*(8), 1222–1241.

Aufdenkampe, A. K., E. Mayorga, P. A. Raymond, J. M. Melack, S. C. Doney, S. R. Alin, R. E. Aalto, and K. Yoo (2011), Riverine coupling of biogeochemical cycles between land, oceans, and atmosphere, *Front. Ecol. Environ.*, *9*(1), 53–60, doi:10.1890/100014.

Battin, T. J., S. Luyssaert, L. A. Kaplan, A. K. Aufdenkampe, A. Richter, and L. J. Tranvik (2009), The boundless carbon cycle, *Nat. Geosci.*, *2*(9), 598–600, doi:10.1038/ngeo618.

Bauer, J. E., W.-J. Cai, P. A. Raymond, T. S. Bianchi, C. S. Hopkinson, and P. A. G. Regnier (2013), The changing carbon cycle of the coastal ocean, *Nature*, *504*(7478), 61–70, doi:10.1038/nature12857.

Beaulieu, J. J., W. D. Shuster, and J. A. Rebholz (2012), Controls on gas transfer velocities in a large river, *J. Geophys. Res.*, *117*, G02007, doi:10.1029/2011JG001794.

Benstead, J. P., and D. S. Leigh (2012), An expanded role for river networks, *Nat. Geosci.*, *5*(10), 678–679.

Borges, A. V., B. Delille, L. S. Schiettecatte, F. Gazeau, G. Abril, and M. Frankignoulle (2004), Gas transfer velocities of CO_2 in three European estuaries (Randers Fjord, Scheldt, and Thames), *Limnol. Oceanogr.*, *49*(5), 1630–1641.

Butman, D., and P. A. Raymond (2011), Significant efflux of carbon dioxide from streams and rivers in the United States, *Nat. Geosci.*, *4*(12), 839–842, doi:10.1038/ngeo1294.

Ciais, P., et al. (2013), Carbon and other biogeochemical cycles, in *Climate Change 2013: The Physical Science Basis. Contribution of Working Group I to the Fifth Assessment Report of the Intergovernmental Panel on Climate Change*, edited by T. F. Stocker et al., Cambridge Univ. Press, Cambridge, U. K., and New York.

CIESIN, and CIAT (2005), *Gridded Population of the World Version 3 (GPWv3): POPULATION Grids* CIESIN, Columbia Univ. New York, Palisades.

Cochonneau, G., et al. (2006), The environmental observation and research project, ORE HYBAM, and the rivers of the Amazon basin, in *Climate Variability and Change—Hydrological Impacts*, vol. 308, edited by S. Demuth et al., pp. 44–50.

Cole, J. J., et al. (2007), Plumbing the global carbon cycle: Integrating inland waters into the terrestrial carbon budget, *Ecosystems*, *10*(1), 171–184, doi:10.1007/s10021-006-9013-8.

Davidson, E. A., R. O. Figueiredo, D. Markewitz, and A. K. Aufdenkampe (2010), Dissolved CO_2 in small catchment streams of eastern Amazonia: A minor pathway of terrestrial carbon loss, *J. Geophys. Res.*, *115*, G04005, doi:10.1029/2009JG001202.

Dawson, J. J. C., C. Bakewell, and M. F. Billett (2001), Is in-stream processing an important control on spatial changes in carbon fluxes in headwater catchments?, *Sci. Total Environ.*, *265*(1–3), 153–167.

Denfeld, B. A., K. E. Frey, W. V. Sobczak, P. J. Mann, and R. M. Holmes (2013), Summer CO_2 evasion from streams and rivers in the Kolyma river basin, north-east Siberia, *Polar Res.*, *32*(SUPPL.).

Denman, K. L., et al. (2007), Couplings between changes in the climate system and biogeochemistry, in *Climate Change 2007: The Physical Science Basis. Contribution of Working Group I to the Fourth Assessment Report of the Intergovernmental Panel on Climate Change*, edited by S. Solomon et al., Cambridge Univ. Press, Cambridge, U. K., and New York.

Dinsmore, K. J., M. F. Billett, and K. E. Dyson (2013), Temperature and precipitation drive temporal variability in aquatic carbon and GHG concentrations and fluxes in a peatland catchment, *Global Change Biol.*, *19*(7), 2133–2148.

Downing, J. A., J. J. Cole, C. M. Duarte, J. J. Middelburg, J. M. Melack, Y. T. Prairie, P. Kortelainen, R. G. Striegl, W. H. McDowell, and L. J. Tranvik (2012), Global abundance and size distribution of streams and rivers, *Inland Waters*, *2*(4), 229–236, doi:10.5268/IW-2.4.502.

Dubois, K. D., D. Lee, and J. Veizer (2010), Isotopic constraints on alkalinity, dissolved organic carbon, and atmospheric carbon dioxide fluxes in the Mississippi River, *J. Geophys. Res.*, *115*, G02018, doi:10.1029/2009JG001102.

Fekete, B. M., C. J. Vörösmarty, and W. Grabs (2002), High-resolution fields of global runoff combining observed river discharge and simulated water balances, *Global Biogeochem. Cycles*, *16*(3), 1042, doi:10.1029/1999GB001254.

Finlay, J. C. (2003), Controls of streamwater dissolved inorganic carbon dynamics in a forested watershed, *Biogeochemistry*, *62*(3), 231–252, doi:10.1023/a:1021183023963.

Friend, A. D., et al. (2014), Carbon residence time dominates uncertainty in terrestrial vegetation responses to future climate and atmospheric CO_2, *Proc. Natl. Acad. Sci. U.S.A.*, *111*(9), 3280–3285, doi:10.1073/pnas.1222477110.

Garcia-Esteves, J., W. Ludwig, P. Kerherve, J. L. Probst, and F. Lespinas (2007), Predicting the impact of land use on the major element and nutrient fluxes in coastal Mediterranean rivers: The case of the Tet River (Southern France), *Appl. Geochem.*, *22*(1), 230–248, doi:10.1016/j.apgeochem.2006.09.013.

Gessler, P. E., O. A. Chadwick, F. Chamran, L. Althouse, and K. Holmes (2000), Modeling soil-landscape and ecosystem properties using terrain attributes, *Soil Sci. Soc. Am. J.*, *64*(6), 2046–2056.

GLOBE-Task-Team, et al. (1999), The Global Land one-kilometer Base Elevation (GLOBE) digital elevation model, Version 1.0. [Available at http://www.ngdc.noaa.gov/mgg/topo/globe.html (Accessed 12 December 2012).]

Gruber, S. (2012), Derivation and analysis of a high-resolution estimate of global permafrost zonation, *Cryosphere*, *6*(1), 221–233, doi:10.5194/tc-6-221-2012.

Hartmann, J., R. Lauerwald, and N. Moosdorf (2014), A brief overview of the GLObal RIver CHemistry Database, GLORICH, *Procedia Earth Planet. Sci.*, *10*, 23–27.

Hess, L. L., J. M. Melack, E. M. L. M. Novo, C. C. F. Barbosa, and M. Gastil (2003), Dual-season mapping of wetland inundation and vegetation for the central Amazon basin, *Remote Sens. Environ.*, *87*(4), 404–428.

Hijmans, R. J., S. E. Cameron, J. L. Parra, P. G. Jones, and A. Jarvis (2005), Very high resolution interpolated climate surfaces for global land areas, *Int. J. Climatol.*, *25*(15), 1965–1978, doi:10.1002/joc.1276.

Hope, D., S. M. Palmer, M. F. Billett, and J. J. C. Dawson (2001), Carbon dioxide and methane evasion from a temperate peatland stream, *Limnol. Oceanogr.*, *46*(4), 847–857.

Humborg, C., C. M. Morth, M. Sundbom, H. Borg, T. Blenckner, R. Giesler, and V. Ittekkot (2010), CO_2 supersaturation along the aquatic conduit in Swedish watersheds as constrained by terrestrial respiration, aquatic respiration and weathering, *Global Change Biol.*, *16*(7), 1966–1978, doi:10.1111/j.1365-2486.2009.02092.x.

Hunt, C. W., J. E. Salisbury, and D. Vandemark (2011), Contribution of non-carbonate anions to total alkalinity and overestimation of $p$$CO_2$ in New England and New Brunswick rivers, *Biogeosciences*, *8*(10), 3069–3076, doi:10.5194/bg-8-3069-2011.

Jenson, S. K. (1991), Applications of hydrologic information automatically extracted from digital elevation models, *Hydrol. Processes*, *5*(1), 31–44.

Johnson, M. S., J. Lehmann, S. J. Riha, A. V. Krusche, J. E. Richey, J. Ometto, and E. G. Couto (2008), CO(2) efflux from Amazonian headwater streams represents a significant fate for deep soil respiration, *Geophys. Res. Lett.*, *35*, L17401, doi:10.1029/2008GL034619.

Kempe, S. (1982), *Long-term Records of CO_2 Pressure Fluctuations in Fresh Waters*, Mitt. Geol.-Paläont. Inst. Univ. Hamburg. SCOPE/UNEP Sonderband, vol. 52, pp. 91–332, Univ. of Hamburg, Hamburg, Germany.

Kempe, S. (1984), Sinks of the anthropogenically enhanced carbon cycle in surface fresh waters, *J. Geophys. Res.*, *89*(ND3), 4657–4676, doi:10.1029/JD089iD03p04657.

Laruelle, G. G., H. H. Dürr, R. Lauerwald, J. Hartmann, C. P. Slomp, N. Goossens, and P. A. G. Regnier (2013), Global multi-scale segmentation of continental and coastal waters from the watersheds to the continental margins, *Hydrol. Earth Syst. Sci.*, *17*(5), 2029–2051, doi:10.5194/hess-17-2029-2013.

Laruelle, G. G., R. Lauerwald, J. Rotschi, P. A. Raymond, J. Hartmann, and P. Regnier (2015), Seasonal response of air-water CO_2 exchange along the land-ocean aquatic continuum of the northeast North American coast, *Biogeosciences*, *12*(5), 1447–1458, doi:10.5194/bg-12-1447-2015.

Lauerwald, R., J. Hartmann, W. Ludwig, and N. Moosdorf (2012), Assessing the nonconservative fluvial fluxes of dissolved organic carbon in North America, *J. Geophys. Res.*, *117*, G01027, doi:10.1029/2011JG001820.

Lauerwald, R., J. Hartmann, N. Moosdorf, S. Kempe, and P. A. Raymond (2013), What controls the spatial patterns of the riverine carbonate system?—A case study for North America, *Chem. Geol.*, *337–338*, 114–127, doi:10.1016/j.chemgeo.2012.11.011.

Lehner, B., and P. Döll (2004), Development and validation of a global database of lakes, reservoirs and wetlands, *J. Hydrol.*, *296*(1–4), 1–22, doi:10.1016/j.jhydrol.2004.03.028.

Lehner, B., K. Verdin, and A. Jarvis (2008), New global hydrography derived from spaceborne elevation data, *Eos Trans. AGU*, *89*(10), 93–94.

Ludwig, W., J. L. Probst, and S. Kempe (1996), Predicting the oceanic input of organic carbon by continental erosion, *Global Biogeochem. Cycles*, *10*(1), 23–41, doi:10.1029/95GB02925.

Lundin, E. J., R. Giesler, A. Persson, M. S. Thompson, and J. Karlsson (2013), Integrating carbon emissions from lakes and streams in a subarctic catchment, *J. Geophys. Res. Biogeosci.*, *118*, 1200–1207, doi:10.1002/jgrg.20092.

Mayorga, E., A. K. Aufdenkampe, C. A. Masiello, A. V. Krusche, J. I. Hedges, P. D. Quay, J. E. Richey, and T. A. Brown (2005), Young organic matter as a source of carbon dioxide outgassing from Amazonian rivers, *Nature*, *436*(7050), 538–541, doi:10.1038/nature03880.

Melack, J. M., R. L. Victoria, and J. Tomasella (2009), Surface waters in Amazonia: Key findings and perspectives, *Geophys. Monogr. Ser.*, *186*, 485–488.

Melching, C. S., and H. E. Flores (1999), Reaeration equations derived from US geological survey database, *J. Environ. Eng. Asce*, *125*(5), 407–414, doi:10.1061/(asce)0733-9372(1999)125:5(407).

Meybeck, M., H. H. Dürr, and C. J. Vörösmarty (2006), Global coastal segmentation and its river catchment contributors: A new look at land-ocean linkage, *Global Biogeochem. Cycles*, *20*, GB1S90, doi:10.1029/2005GB002540.

Miralles, D. G., T. R. H. Holmes, R. A. M. De Jeu, J. H. Gash, A. G. C. A. Meesters, and A. J. Dolman (2011), Global land-surface evaporation estimated from satellite-based observations, *Hydrol. Earth Syst. Sci.*, *15*(2), 453–469, doi:10.5194/hess-15-453-2011.

O'Connor, D., and W. Dobbins (1958), Mechanism of reaeration in natural streams, *Trans. Am. Soc. Civ. Eng.*, *123*, 641–684.

Owens, M., R. W. Edwards, and J. W. Gibbs (1964), Some reaeration studies in streams, *Air Water Pollut.*, *8*(8–9), 469–486.

Park, P. K., L. I. Gordon, S. W. Hager, and M. C. Cissell (1969), Carbon dioxide partial pressure in the Columbia River, *Science*, *166*(3907), 867–868.

Parkhurst, D. L., and C. A. J. Appelo (1999), User's guide to PHREEQC (v2)—A computer program for speciation, batch-reaction, one-dimensional transport, and inverse geochemical calculations, edited by USGS, *Water Resour. Invest. Rep.*, *99–4259*.

PARTNERS-Project-Group (2009), PARTNERS Project Arctic River Biogeochemistry Data Set Version 1.1. [Available at http://www.arcticgreat-rivers.org/data.html.]

Prigent, C., F. Papa, F. Aires, W. B. Rossow, and E. Matthews (2007), Global inundation dynamics inferred from multiple satellite observations, 1993–2000, *J. Geophys. Res.*, *112*, D12107, doi:10.1029/2006JD007847.

R Core Team (2013), R: A language and environment for statistical computing. [Available at http://www.r-project.org.]

Rasera, M., et al. (2008), Small rivers in the southwestern Amazon and their role in CO_2 outgassing, *Earth Interact.*, *12*(6), doi:10.1175/2008ei257.1.

Rasera, M. F. F. L., A. V. Krusche, J. E. Richey, M. V. R. Ballester, and R. L. Victória (2013), Spatial and temporal variability of pCO_2 and CO_2 efflux in seven Amazonian Rivers, *Biogeochemistry*, *116*(1–3), 241–259.

Rawlins, B. G., B. Palumbo-Roe, D. C. Gooddy, F. Worrall, and H. Smith (2014), A model of potential carbon dioxide efflux from surface water across England and Wales using headwater stream survey data and landscape predictors, *Biogeosciences*, *11*(7), 1911–1925, doi:10.5194/bg-11-1911-2014.

Raymond, P. A., C. J. Zappa, D. Butman, T. L. Bott, J. Potter, P. Mulholland, A. E. Laursen, W. H. McDowell, and D. Newbold (2012), Scaling the gas transfer velocity and hydraulic geometry in streams and small rivers, *Limnol. Oceanogr. Fluids Environ.*, *2*, 41–53, doi:10.1215/21573689-1597669.

Raymond, P. A., et al. (2013), Global carbon dioxide emissions from inland waters, *Nature*, *503*(7476), 355–359, doi:10.1038/nature12760.

Regnier, P., et al. (2013), Anthropogenic perturbation of the carbon fluxes from land to ocean, *Nat. Geosci.*, *6*(8), 597–607, doi:10.1038/ngeo1830.

Richey, J. E., J. I. Hedges, A. H. Devol, P. D. Quay, R. Victoria, L. Martinelli, and B. R. Forsberg (1990), Biogeochemistry of carbon in the Amazon River, *Limnol. Oceanogr.*, *35*(2), 352–371, doi:10.4319/lo.1990.35.2.0352.

Richey, J. E., J. M. Melack, A. K. Aufdenkampe, V. M. Ballester, and L. L. Hess (2002), Outgassing from Amazonian rivers and wetlands as a large tropical source of atmospheric CO_2, *Nature*, *416*(6881), 617–620, doi:10.1038/416617a.

Strahler, A. N. (1952), Hypsometric (area-altitude) analysis of erosional topology, *Geol. Soc. Am. Bull.*, *63*(11), 1117–1142, doi:10.1130/0016-7606(1952)63[1117:HAAOET]2.0.CO;2.

Striegl, R. G., M. M. Dornblaser, C. P. McDonald, J. R. Rover, and E. G. Stets (2012), Carbon dioxide and methane emissions from the Yukon River system, *Global Biogeochem. Cycles*, *26*, doi:10.1029/2012GB004306.

Telmer, K., and J. Veizer (1999), Carbon fluxes, pCO_2 and substrate weathering in a large northern river basin, Canada: Carbon isotope perspectives, *Chem. Geol.*, *159*(1–4), 61–86.

Teodoru, C. R., P. A. Del Giorgio, Y. T. Prairie, and M. Camire (2009), Patterns in pCO_2 in boreal streams and rivers of northern Quebec, Canada, *Global Biogeochem. Cycles*, *23*, GB2012, doi:10.1029/2008GB003404.

Tranvik, L. J., et al. (2009), Lakes and reservoirs as regulators of carbon cycling and climate, *Limnol. Oceanogr.*, *54*(6), 2298–2314, doi:10.4319/lo.2009.54.6_part_2.2298.

USGS-EROS-Center (2000), HYDRO1k elevation derivative database. [Available at https://lta.cr.usgs.gov/HYDRO1K (Accessed 20 December 2012).]

Vanderborght, J. P., R. Wollast, M. Loijens, and P. Regnier (2002), Application of a transport-reaction model to the estimation of biogas fluxes in the Scheldt estuary, *Biogeochemistry*, *59*(1–2), 207–237, doi:10.1023/a:1015573131561.

Vanderborght, J. P., I. M. Folmer, D. R. Aguilera, T. Uhrenholdt, and P. Regnier (2007), Reactive-transport modelling of C, N, and O-2 in a river-estuarine-coastal zone system: Application to the Scheldt estuary, *Mar. Chem.*, *106*(1–2), 92–110, doi:10.1016/j.marchem.2006.06.006.

Wallin, M. B., M. G. Öquist, I. Buffam, M. F. Billett, J. Nisell, and K. H. Bishop (2011), Spatiotemporal variability of the gas transfer coefficient (<emph typeK CO_2) in boreal streams: Implications for large scale estimates of CO_2 evasion, *Global Biogeochem. Cycles*, *25*, GB3025, doi:10.1029/2010GB003975.

Wallin, M. B., T. Grabs, I. Buffam, H. Laudon, A. Ågren, M. G. Öquist, and K. Bishop (2013), Evasion of CO_2 from streams—The dominant component of the carbon export through the aquatic conduit in a boreal landscape, *Global Change Biol.*, *19*(3), 785–797.

Wallin, M. B., S. Löfgren, M. Erlandsson, and K. Bishop (2014), Representative regional sampling of carbon dioxide and methane concentrations in hemiboreal headwater streams reveal underestimates in less systematic approaches, *Global Biogeochem. Cycles*, *28*, 465–479, doi:10.1002/2013GB004715.

Wang, F. S., Y. Wang, J. Zhang, H. Xu, and X. Wei (2007), Human impact on the historical change of CO_2 degassing flux in River Changjiang, *Geochem. Trans.*, *8*, doi:10.1186/1467-4866-8-7.

Wang, Z. A., D. J. Bienvenu, P. J. Mann, K. A. Hoering, J. R. Poulsen, R. G. M. Spencer, and R. M. Holmes (2013), Inorganic carbon speciation and fluxes in the Congo River, *Geophys. Res. Lett.*, *40*, 511–516, doi:10.1002/grl.50160.

Ward, N. D., R. G. Keil, P. M. Medeiros, D. C. Brito, A. C. Cunha, T. Dittmar, P. L. Yager, A. V. Krusche, and J. E. Richey (2013), Degradation of terrestrially derived macromolecules in the Amazon River, *Nat. Geosci.*, *6*(7), 530–533.

Worrall, F., T. P. Burt, J. G. Rowson, J. Warburton, and J. K. Adamson (2009), The multi-annual carbon budget of a peat-covered catchment, *Sci. Total Environ.*, *407*(13), 4084–4094, doi:10.1016/j.scitotenv.2009.03.008.

Zhao, M., F. A. Heinsch, R. R. Nemani, and S. W. Running (2005), Improvements of the MODIS terrestrial gross and net primary production global data set, *Remote Sens. Environ.*, *95*(2), 164–176, doi:10.1016/j.rse.2004.12.011.